Picosecond Studies of Proton Transfer in Clusters. 2. Dynamics and Energetics of Solvated Phenol Cation

Jhobe Steadman† and Jack A. Syage*

Contribution from the Aerophysics Laboratory, The Aerospace Corporation, P.O. Box 92957/M5-754, Los Angeles, California 90009. *Received March 28, 1991*

Abstract: The dissociative proton transfer (DPT) of the phenol cation was studied in molecular clusters of NH_3, CH_3OH, H_2O, and other hydrogen-bonding solvents. These studies confirm the existence of a double well reaction coordinate and lead to estimates of the activation energy, enthalpy, and shape of the potential curves as a function of solvent cluster size. By using two-color picosecond excitation and delayed ionization from an excited neutral proton transfer state, cluster ions were produced nearly exclusively in either the strongly bound inner well or the shallow and extended outer well. We have measured very different reaction efficiencies from these two potential wells. Potential energy surfaces are constructed for stepwise solvation that predict the existence of a double well reaction coordinate and explain the origin of the activation barrier. Upper limits to the barrier height for $(NH_3)_n$ solvation range from about 1.5 (n = 1) to 1.0 eV (n = 4). The gas-phase bimolecular energy barrier relative to the separated reactant molecules is about 0.6 eV.

1. Introduction

The study of chemical reactions in clusters provides an incisive probe of the energetics of solvation on a single-molecule basis. Recent studies have shown that just a few solvent molecules can exert a profound influence on the outcome of unimolecular and bimolecular reactions in clusters.[1-15] In some cases the addition of a single solvent molecule to a small cluster can "switch on" a chemical reaction. Acid–base proton-transfer reactions are prevalent in solution,[16-20] yet they are quite rare in the gas phase.[21-23] One would expect studies in molecular clusters to provide a direct connection between gas-phase and condensed-phase properties and help answer fundamental questions such as when does a reactive molecule become solvated?

The extent to which proton transfer or acid–base chemistry occurs in clusters or solution depends critically on how well the solvent stabilizes the proton. In a previous paper (paper 1),[12] we investigated the excited-state proton transfer (ESPT) from the locally excited S_1 state to ion-pair states of phenol. In this paper, we examine proton transfer in the *ionic* clusters. Kebarle and co-workers are among the originators in studies of stepwise solvation of ion–molecule reactions.[1,2] Their work, which used high-pressure flow tube reactors, has led to an important body of data on solvation energies for cluster ions, particularly for protonated ions. More recently, molecular beams have been used to study chemistry in clusters with techniques such as electron-impact ionization/fragmentation to study cluster ion–molecule reactions[3,4] and resonance-enhanced multiphoton ionization (REMPI) to study neutral and ionic cluster chemistry.[5-14] Techniques have also been employed to mass-select cluster ions before subjecting them to photochemical excitation.[24-26] Recently, time-resolved spectroscopy has been employed to study rates of cluster reactions.[10-15] In the present work, we use delayed picosecond pump-probe excitation to access very different regions of the cluster ion Franck–Condon surface, thus revealing detailed properties of the reactive potential energy surface.

The present investigation focuses on an important property observed for proton-transfer reactions in gas-phase biomolecular ion–molecule collisions. Proton transfer involving ions with localized charge normally occurs with near unit collision efficiency, whereas ions with delocalized charge (e.g., aromatic cations) react far more slowly, despite large exothermicities. These observations led Brauman and co-workers to postulate a double minima reaction coordinate for the latter reactions, although direct evidence has never been obtained.[27,28] Ionization of van der Waals (vdW) complexes allows one to study ion–molecule reactions starting from a potential minimum. Mikami et al. reported that the bound complex $PhOH^+\cdots NH_3$ fails to undergo dissociative proton transfer (DPT) to $PhO + NH_4^+$ at energies up to and exceeding 1 eV above the ion minimum, yet the nearly equienergetic dissociation to form

† National Research Council postdoctoral associate.

(1) (a) Kebarle, P. *Ann. Rev. Phys. Chem.* **1977**, *28*, 445. (b) Grimsrud, E. P.; Kebarle, P. *J. Am. Chem. Soc.* **1973**, *95*, 7939. (c) Payzant, J. D.; Cunningham, A. J.; Kebarle, P. *Can. J. Chem.* **1973**, *51*, 3242.
(2) (a) Hogg, A. M.; P. Kebarle *J. Chem. Phys.* **1965**, *43*, 449. (b) Searles, S. K.; Kebarle, P. *J. Phys. Chem.* **1968**, *72*, 742.
(3) (a) Garvey, J. F.; Peifer, W. R.; Coolbaugh, M. T. *Acct. Chem. Res.* **1991**, *24*, 48. (b) Stace, A. J. *J. Am. Chem. Soc.* **1985**, *107*, 755. (c) Stace, A. J.; Moore, C. *J. Am. Chem. Soc.* **1983**, *105*, 1814.
(4) (a) Shinohara, H.; Nishi, N. *Chem. Phys. Lett.* **1982**, *87*, 561. (b) Shinohara, H.; Nishi, N.; Washida, N. *Chem. Phys. Lett.* **1984**, *106*, 302. (c) Shinohara, H.; Nishi, N.; Washida, N. *J. Chem. Phys.* **1985**, *83*, 1939.
(5) (a) Breen, J. J.; Tzeng, W.-B.; Kilgore, K.; Keesee, R. G.; Castleman, A. W., Jr. *J. Chem. Phys.* **1989**, *90*, 19. (b) Echt, O.; Dao, P. D.; Morgan, S.; Castleman, A. W., Jr. *J. Chem. Phys.* **1985**, *82*, 4076. (c) Morgan, S.; Castleman, A. W., Jr. *J. Am. Chem. Soc.* **1987**, *109*, 2867.
(6) Brutschy, D.; Janes, D.; Eggert, J. *Ber. Bunsenges, Phys. Chem.* **1988**, *92*, 74.
(7) (a) Cheshnovsky, O.; Leutwyler, S. *J. Chem. Phys.* **1988**, *88*, 4127. (b) Droz, T.; Knochenmuss, R.; Leutwyler, S. *J. Chem. Phys.* **1990**, *93*, 4520. (c) Knochenmuss, R.; Cheshnovsky, O.; Leutwyler, S. *Chem. Phys. Lett.* **1988**, *144*, 317.
(8) (a) Jouvet, C.; Lardeux-Dedonder, C.; Richard-Viard, M.; Solgadi, D.; Tramer, A. *J. Phys. Chem.* **1990**, *94*, 5041. (b) Solgadi, D.; Jouvet, C.; Tramer, A. *J. Phys. Chem.* **1988**, *92*, 3313.
(9) (a) Syage, J. A. *J. Chem. Phys.* **1990**, *92*, 1804. (b) Syage, J. A. *J. Phys. Chem.* **1989**, *93*, 107.
(10) Syage, J. A.; Steadman, J. *Chem. Phys. Lett.* **1990**, *166*, 159.
(11) Steadman, J.; Syage, J. A. *J. Chem. Phys.* **1990**, *92*, 4630.
(12) Syage, J. A.; Steadman, J. *J. Chem. Phys.*, in press.
(13) (a) Syage, J. A. *SPIE Proc.* **1990**, *1209*, 64. (b) Steadman, J.; Fournier, E. W.; Syage, J. A. *Appl. Opt.* **1990**, *29*, 4962. (c) Steadman, J.; Syage, J. A. *J. Phys. Chem.*, in press.
(14) (a) Breen, J. J.; Peng, L. W.; Willberg, D. M.; Heikal, A.; Cong, P.; Zewail, A. H. *J. Chem. Phys.* **1990**, *92*, 805. (b) Breen, J. J.; Willberg, D. M.; Gutman, M.; Zewail, A. H. *J. Chem. Phys.* **1990**, *93*, 9180.
(15) (a) Ray, D.; Levinger, N. E.; Papanikolas, J. M.; Lineberger, W. C. *J. Chem. Phys.* **1989**, *91*, 6533. (b) Cassasa, M. P.; Stephenson, J. C.; King, D. S. *J. Chem. Phys.* **1988**, *89*, 1966. (c) Wittmeyer, S. A.; Kazlshka, A. J.; Topp, M. R. *Chem. Phys. Lett.* **1989**, *154*, 1.
(16) Kosower, E. M.; Huppert, D. *Annu. Rev. Phys. Chem.* **1986**, *37*, 127.
(17) (a) Smith, K. K.; Kaufmann, K. J.; Huppert, D.; Gutman, M. *Chem. Phys. Lett.* **1979**, *64*, 522. (b) Shizuka, H.; Tsutsumi, K.; Takeuchi, H.; Tanaka, I. *Chem. Phys. Lett.* **1979**, *62*, 408. (c) Rentzepis, P. M.; Barbara, P. F. *Adv. Chem. Phys.* **1981**, *47*, 627.
(18) (a) Pines, E.; Huppert, D.; Agmon, N. *J. Chem. Phys.* **1988**, *88*, 5620. (b) Huppert, D. H.; Jayaraman, A.; Maines, R. G., Sr.; Steyert, D. W.; Rentzepis, P. M. *J. Chem. Phys.* **1984**, *81*, 5596.
(19) (a) Webb, S. P.; Philips, L. A.; Yeh, S. W.; Tolbert, L. M.; Clark, J. H. *J. Phys. Chem.* **1986**, *90*, 5154. (b) Lee, J.; Griffin, R. D.; Robinson, G. W. *J. Chem. Phys.* **1985**, *82*, 4920.
(20) (a) Turro, N. J. *Modern Molecular Photochemistry*; Benjamin/Cummings: Reading, MA, 1978. (b) Lowry, T. H.; Richardson, K. S. *Mechanism and Theory in Organic Chemistry*; Harper and Row: New York, 1970.
(21) Moylan, C. R.; Brauman, J. I. *Ann. Rev. Phys. Chem.* **1983**, *34*, 187.
(22) Adams, N. G.; Smith, D.; Paulson, J. F. *J. Chem. Phys.* **1980**, *72*, 288.

0002-7863/91/1513-6786$02.50/0

$PhOH^+ + NH_3$ clearly occurs at these energies.[29] These results suggest the presence of a reaction barrier to DPT.

We report on the structure and properties of the reactive complex in the outer potential well and provide an explanation for the origin of the reactive barrier. The direct detection of this complex is achieved by a two-step picosecond ionization process shown in Figure 1. By timing the ionization from a reactive intermediate neutral state, we can excite directly and specifically into either cluster-ion potential well. We have measured dissociation fractions from both potential wells as a function of ion energies, which enables us to (1) establish the presence of a reactive barrier, (2) explain the origin of the barrier and transition state, and (3) show how the reaction coordinate evolves by progressive solvation from the gas-phase ion–molecule limit to the bulk-solvation limit. These results, together with literature data, have enabled us to present a picture of the evolution of gas-phase to condensed-phase chemistry from the viewpoint of bimolecular reactive scattering, reducing the problem to the most relevant reactant and solvent coordinates.

2. Experimental Section

The molecular beam time-of-flight (TOF) mass spectrometer and data acquisition system have been described before.[9] Typical pulsed expansion conditions were 35-psi He or Ar, 500-μm diameter nozzle, 400-μs pulse width, 2-cm nozzle-skimmer distance, and 1-mm diameter skimmer. The ambient base pressure in the ionization chamber was typically 2×10^{-8} Torr, rising to about 2×10^{-7} Torr during operation of the pulsed nozzle at 10 Hz. The ion optics consist of the conventional three-grid configuration as well as a pulsed electron impact (EI) ionization source described in detail elsewhere.[26a,30] Solvated aromatic clusters were prepared by a variety of procedures. In most cases, the aromatic was deposited in a sample holder contained in the temperature-controlled pulsed nozzle typically maintained at about 60 °C. For ammonia solvation, a 2-L high-pressure cylinder was filled with 10% ammonia in helium. Water, methanol, and hydrazine solvation was achieved by passing the helium flow through a bubbler containing either of these solvents. The extent of clustering is very sensitive to the relative delay between the laser pulse and the pulsed valve firing. For example, by exciting within 25–50 μs of the gas pulse extremities, where the expansion is warmer, it is possible to suppress formation of larger clusters and form predominantly the single-solvated cation. Studies of larger clusters are achieved by exciting toward the colder central region of the gas pulse. The cluster distribution is fairly constant over the middle 200–300 μs region of a nominal 400 μs pulse. The internal cluster temperatures are not known; however, our conditions are very stable judging by the reproducibility of all experimental results, including rate measurements, on a day-to-day basis.

A pulsed (10 Hz) active/passive mode-locked and amplified Nd:YAG laser was used to produce frequency doubled (532 nm, 25 ps), tripled (355 nm, 25 ps), and quadrupled (266 nm, 18 ps) output and to pump a short-cavity tunable dye laser (10 ps).[12,13] The pump excitation λ_1 was provided by 266-nm pulses. The probe excitation λ_2 was supplied by either the 532- or 355-nm Nd:YAG harmonics. The λ_1 and the λ_2 pulses traveled along separate variable delay lines and were then combined with a dichroic beamsplitter and directed collinearly into the molecular beam apparatus. Polarizing attenuators and neutral density filters were used to reduce pulse energies. Time-resolved spectra for the sequence $\lambda_1 - t - \lambda_2$ were recorded by varying t with a scanning optical delay line. The measured sum-frequency cross correlation signal for the two pulses gave a Gaussian-shaped response with a typical width of 25–30 ps (FWHM). Calculated curves were fitted to the data by convolving with the instrument response function.

TOF mass spectra were recorded by digitizing the amplified current output of a dual microchannel plate detector at a 100-MHz sampling rate. Time-resolved measurements were recorded by integrating specific ion-mass signals with a boxcar averager while scanning the picosecond delay line.

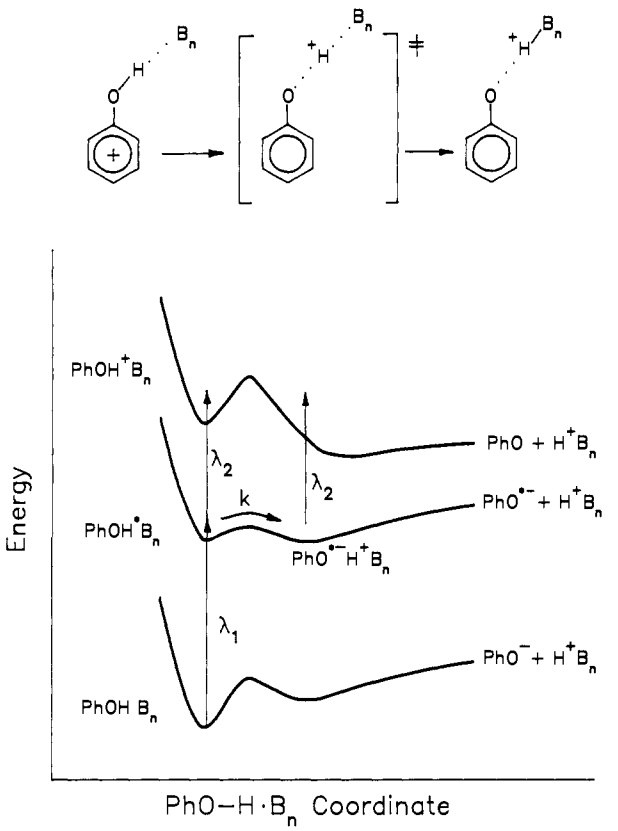

Figure 1. Energy diagram for $PhOH(NH_3)_n$ consistent with a cluster size of $n \sim 5$. Excitation scheme showing how delayed ionization by λ_2 can produce cluster ions in the outer potential well for reactive $PhOH^*B_n$ clusters excited by λ_1. The λ_2 ionization may occur by more than one photon. Pictorial electronic structures are given for the inner well, transition-state, and outer well complexes.

3. Results and Analysis

We represent dissociative proton transfer (DPT) in solvated cluster ions by the following reaction

$$[AH]^+B_n \rightarrow A + H^+B_n$$

where $[AH]^+$ is the acid and n is the number of base solvent molecules B in the cluster. (We use brackets for $[AH]^+$ to indicate that the charge is not necessarily on the H atom, which is an important point.) Cluster ions are formed in this study by picosecond pump-delay-probe REMPI through an excited neutral state of phenol (henceforth PhOH). A representative potential energy diagram and the excitation scheme is given in Figure 1. The details of the ion potential energy curves and how they vary with cluster size are discussed in section 5. In the excited S_1 electronic state, solvated phenol can undergo a proton transfer depending on the properties of the solvent cluster B_n (e.g., aggregate proton affinity or basicity). Proton charge transfer from the S_1 state of PhOH to $(NH_3)_n$ solvent clusters occurs only for sizes $n > 4$ with a time constant of 60–70 ps (cf. paper 1).[12] We show here that the reactant S_1 state ionizes to the inner potential well of the cluster ion, whereas the product ion-pair state ionizes to the outer potential well (Figure 1). Consequently, by varying the delay time of the probe pulse, one can control the proportion of ions formed on either side of the ion barrier.

Most of the results and discussion focus on PhOH chemistry in the relatively strong base cluster $(NH_3)_n$. Other solvent

(23) *Gas Phase Ion Chemistry*; Bowers, M. T., Ed.; Academic Press: New York, 1979; Vols. I and II.
(24) Alexander, M. L.; Levinger, N. E.; Johnson, M. A.; Ray, D.; Lineberger, W. C. *J. Chem. Phys.* **1988**, *88*, 6200.
(25) (a) Bloomfield, L. A.; Freeman, R. R.; Brown, W. L. *Phys. Rev. Lett.* **1985**, *54*, 2246. (b) Zhang, Q.-L.; Liu, Y.; Curl, R. F.; Tittel, F. K.; Smalley, R. E. *J. Chem. Phys.* **1988**, *88*, 1670. (c) Alexander, M. L.; Johnson, M. A.; Levinger, N. E.; Lineberger, W. C. *Phys. Rev. Lett.* **1986**, *57*, 976.
(26) (a) Syage, J. A.; Steadman, J. *Rev. Sci. Instrum.* **1990**, *61*, 1204. (b) Beck, S. M.; Andrews, J. *J. Chem. Phys.* **1989**, *91*, 4420. (c) LaiHing, K.; Chen, P. Y.; Taylor, T. G.; Willey, K. F.; Peschke, M.; Duncan, M. A. *Anal. Chem.* **1989**, *61*, 1458.
(27) (a) Moylan, C. R.; Brauman, J. I. *Annu. Rev. Phys. Chem.* **1983**, *34*, 187. (b) Comita, P. B.; Brauman, J. I. *Science* **1985**, *227*, 863.
(28) (a) Farneth, W. E.; Brauman, J. I. *J. Am. Chem. Soc.* **1976**, *98*, 7891. (b) Jasinski, J. M.; Brauman, J. I. *J. Am. Chem. Soc.* **1980**, *102*, 2906.
(29) Mikami, N.; Okabe, A.; Suzuki, I. *J. Phys. Chem.* **1988**, *92*, 1858.
(30) (a) Syage, J. A. *Chem. Phys. Lett.* **1988**, *143*, 19. (b) Syage, J. A.; Pollard, J. E.; Steadman, J. *Chem. Phys. Lett.* **1989**, *161*, 103.

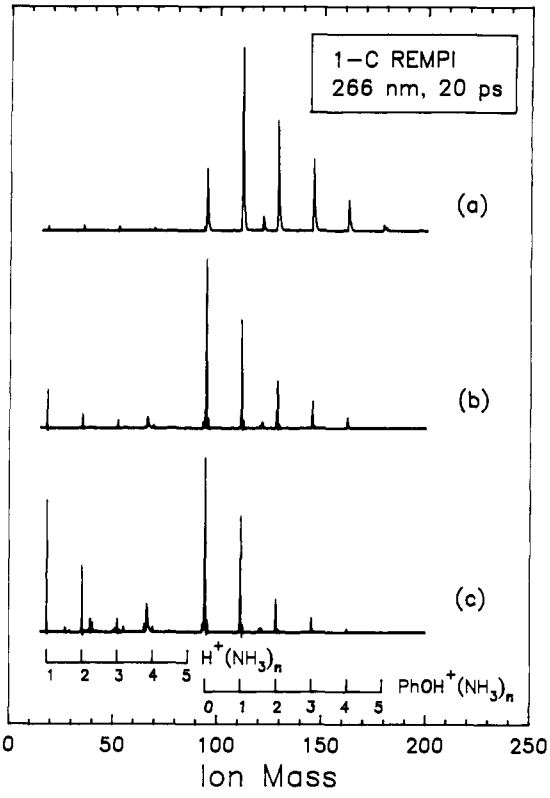

Figure 2. One-color picosecond REMPI mass spectra with 20-ps 266-nm radiation of varying pulse intensity: (a) two-photon signals (~20 μJ/pulse, 2-mm diameter), (b) appearance of $H^+(NH_3)_n$ at the three-photon level (~80 μJ/pulse, 2-mm diameter), (c) appearance of aromatic fragments at the four-plus photon level (~80 μJ/pulse, ~300-μm diameter). Deflector voltage was adjusted to emphasize lower masses.

molecules studied include H_2O, CH_3OH, $N(CH_3)_3$, and N_2H_4; these results will enter into the discussion. We report on the dissociative proton transfer reaction

$$[PhOH]^+(NH_3)_n \rightarrow PhO + H^+(NH_3)_{n-m} + mNH_3$$

with the interest of obtaining the barrier height and heat of reaction as a function of cluster size. We also discuss the role of evaporation.

Inner Potential Well Ionization. $[PhOH]^{*+}B_n$ clusters are produced in the inner potential well (Figure 1) for an ionization delay time of $t = 0$. We examine 266-nm one-color (1-C) picosecond REMPI mass spectra as a function of pulse energy in Figure 2. At low power (Figure 2a) a cluster distribution is observed with little evidence of DPT or fragmentation. It is believed that this spectrum is dominated by two-photon ionization without further absorption of photons by the cluster ions. DPT products were also absent when using the solvents H_2O and CH_3OH under similar conditions. Some evaporation in $[PhOH]^+(NH_3)_n$ occurs, but it is not extensive judging by the weakness of the $n = 0$ signal relative to $n = 1$. By increasing the pulse energy (Figure 2b) a series of $H^+(NH_3)_n$ DPT peaks appear due to absorption of a photon by the parent cluster ions (three-photon total energy). At even higher power (Figure 2c), the DPT products become more prominent and aromatic fragmentation begins to appear, the latter presumably due to a four- (or more) photon process.

The results of Figure 2 indicate that a large barrier to DPT exists from the inner potential well. The two-photon energy of 9.32 eV exceeds the ionization potentials of the clusters by energies ranging from 1.47 ($n = 1$) to 2.40 eV ($n = 4$). Naturally, the amount of energy that ends up in the cluster ions will be less, depending on the Franck–Condon factors for ionization. An estimate of the barrier heights is made in section 5.

Outer Well Ionization/Dissociation. The rate of ESPT following 266-nm excitation of $PhOH(NH_3)_n$ to the S_1 electronic state is

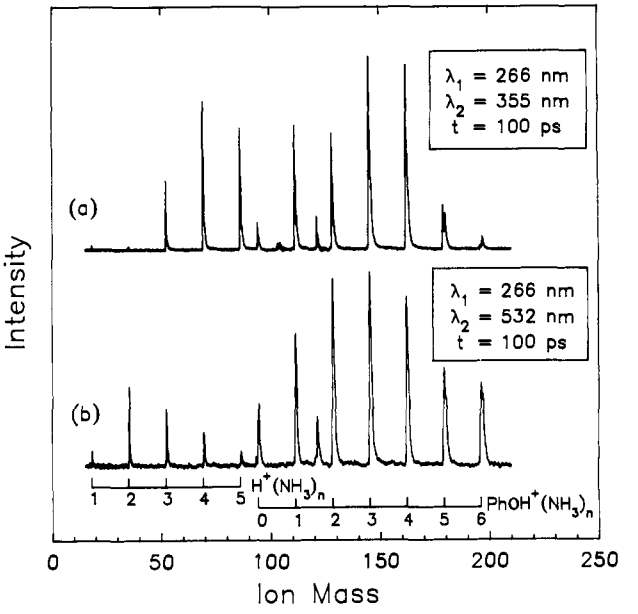

Figure 3. Two-color picosecond delayed ionization REMPI mass spectra for (a) λ_2 = 355-nm, one-photon ionization and (b) λ_2 = 532-nm, two-photon ionization. Excitation conditions were λ_1 = 266 nm (~20 μJ/pulse, 2-mm diameter), λ_2 = 355 nm (~0.5 mJ/pulse, 3-mm diameter), and λ_2 = 532 nm (~1 mJ/pulse, 3-mm diameter). Expansion conditions were 10% NH_3 in He at 35 psi and phenol at 60 °C. The signal at 121 amu is believed to be an impurity. Deflection plates were adjusted to emphasize lower masses.

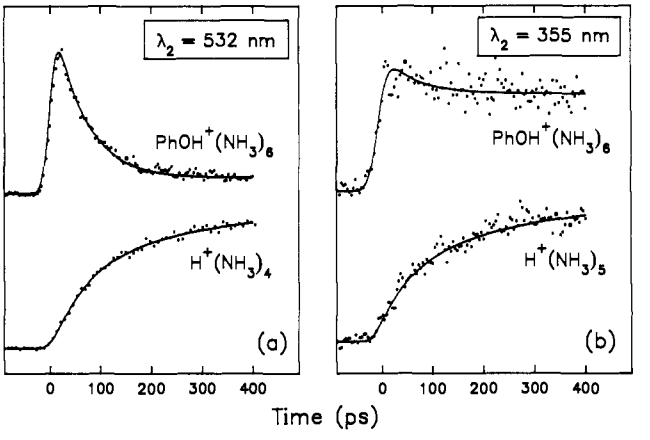

Figure 4. Time-resolved measurements of reactant $[PhOH]^+(NH_3)_n$ (R^+) and product $H^+(NH_3)_n$ (P^+) signals for cluster size $n = 6$: (a) λ_2 = 532-nm, two-photon ionization and (b) λ_2 = 355-nm, one-photon ionization. We show $H^+(NH_3)_4$ traces for $n = 4$ and $n = 5$ because, typically, two and one solvent molecules evaporate at these respective ionization energies following DPT (ref 13b). The R^+ data were fitted to eq 1 for $1/k$ = 65 ps, $f_a = 0$, $i_a/i_b = 2.0$, and $f_b = 0.96$ (λ_2 = 532 nm) and 0.65 (λ_2 = 355 nm). The P^+ data were fitted to a double exponential function (described in paper 1, ref 12) with time constants 65 and 350 ps.

$1/k \simeq 60$–70 ps for solvent cluster sizes of $n > 4$.[11,12] Choosing a pump-probe delay time $t > 1/k$ allows selective ionization to the outer potential well for these larger cluster sizes. Two-color (2-C) delayed ionization mass spectra are presented in Figure 3 for total photon energy equal to or less than that used for recording Figure 2a. The extent of dissociation from the outer well is striking. For λ_2 = 355-nm ionization (8.15 eV total photon energy), a strong series of $H^+(NH_3)_n$ peaks are observed beginning at $n = 3$ (Figure 3a). (Some evaporation occurs in the course of dissociation; however, very little product ion signal is observed for cluster sizes $n < 3$.) The smaller clusters fail to undergo S_1 proton transfer and are ionized into the strongly bound inner potential well. A series of $H^+(NH_3)_n$ DPT signals is also observed with λ_2 = 532-nm ionization[31] (Figure 3b). In this case two

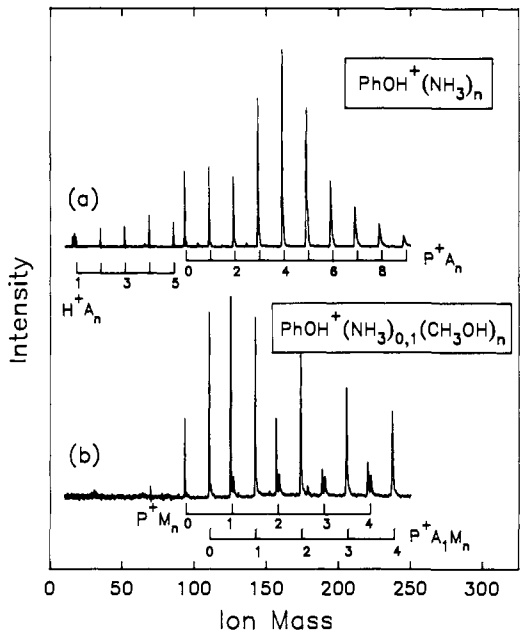

Figure 5. One-color nanosecond REMPI mass spectra at 280 nm: (a) pure $(NH_3)_n$ solvation and (b) mixed solvation involving $NH_3(CH_3OH)_n$. P = phenol, A = NH_3, and M = CH_3OH. The peaks that appear at 2 amu above the P^+M_n series are presumed to be due to demethylation (loss of 15 amu) from $P^+A_1M_n$ cluster ions.

photons are absorbed in the ionization process, hence, evaporation is more extensive.

The time-resolved measurements establish that the products $H^+(NH_3)_n$ occur by DPT from the outer potential well and not the inner well. We present measurements of $PhOH^*(NH_3)_n$ reactant decay (by detecting $[PhOH]^{*+}(NH_3)_n$) and $PhO^{*-}H^+(NH_3)_n$ product formation (by detecting $H^+(NH_3)_n$) in Figure 4. The $[PhOH]^{*+}(NH_3)_n$ signal decays to the baseline when using 532-nm two-photon ionization (Figure 4a), indicating that ionization to the outer well from the neutral ion-pair state (Figure 1) is nearly completely dissociative, leading to $H^+(NH_3)_n$. The growth rate of the $H^+(NH_3)_n$ signal matches the decay rate of the $[PhOH]^+(NH_3)_n$ signal. When using 355-nm one-photon ionization (Figure 4b), the reactant ion yield does not change significantly with t, indicating that DPT from the outer potential well is less extensive at this lower ionization energy. Dissociation is still significant, as seen by the prominent $H^+(NH_3)_n$ signals in Figure 3a and the formation kinetics in Figure 4b. The calculated curves in Figure 4 are based on a model described in the following section that enables one to determine the dissociation quantum yields from both the inner and outer well as a function of cluster size.

Our studies of phenol cation in the less basic solvent cluster $(CH_3OH)_n$ provide further evidence that an outer well cluster ion structure is responsible for DPT. The lifetimes of S_1-excited $PhOH^*(CH_3OH)_n$ clusters are ≥ 10 ns (measured for $n \leq 11$).[12] Because CH_3OH is a weaker base than NH_3 (gas-phase proton affinities of 7.90 and 8.84 eV, respectively),[32] ESPT does not occur in this solvent for moderate cluster sizes. Indeed, the DPT-protonated solvent signal H^+B_n is absent for $(CH_3OH)_n$ and for mixed $NH_3(CH_3OH)_n$ solvent clusters, yet it is present for pure $(NH_3)_n$ solvation (Figure 5). These results indicate that H^+B_n is produced by dissociative ionization from the excited ion-pair state.

4. Model for Delayed Ionization/Dissociation

The measured time-resolved yields of ionization and dissociation from the inner and outer wells (Figure 4) can be modeled by a set of rate equations that assumes the following steps

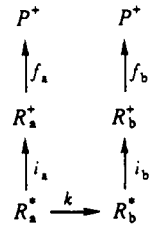

The undissociated cluster ion signal $[PhOH]^+B_n$ is designated by R^+ (= $R_a^+ + R_b^+$), and the dissociated product signal H^+B_n is designated by P^+. We distinguish the inner and outer potential well species, R_a^+ and R_b^+, respectively, even though the mass spectrum only measures the sum R^+. R_a^* and R_b^* refer to the locally excited S_1 and the ion-pair excited neutral states, respectively (Figure 1). The ionization efficiencies from the locally excited S_1 and the ion-pair states are denoted by i_a and i_b, and the fractions of dissociation from the inner and outer potential well are represented by f_a and f_b, respectively. The rate constant k = (60–70 ps)$^{-1}$ was measured previously.[11,12] This model does not include processes that occur on a time scale much longer than $1/k$, such as radiationless decay from R_a^* and R_b^* and solvent reorganization from R_b^*. The solution of the rate equations for R^+ and P^+ are given by

$$R^+(t) = R_0^*\{i_b(1 - f_b) + [i_a(1 - f_a) - i_b(1 - f_b)]e^{-kt}\} \quad (1)$$

$$P^+(t) = R_0^*\{i_b f_b + [i_a f_a - i_b f_b]e^{-kt}\} \quad (2)$$

where R_0^* is a proportionality constant based on the initial quantity of neutral S_1 excited-state clusters $PhOH^*B_n$. The sum of these equations

$$R^+(t) + P^+(t) = R_0^*\{i_b + [i_a - i_b]e^{-kt}\} \quad (3)$$

allows a determination of the relative values of i_a and i_b. If reactant and product ionization involve the same number of photons, then the ratio of i_a and i_b is equivalent to the ratio of ionization cross sections σ_a and σ_b.

We highlight a few experimental observations: (1) the mass spectrum in Figure 2a, corresponding to inner well ionization, shows very little dissociation ($f_a \ll 1$); (2) the trace for $R^+(t)$ in Figure 4a decays to the baseline, indicating nearly complete dissociation in the outer well ($f_b \sim 1$) for λ_2 = 532-nm two-photon ionization; (3) the analogous decay in Figure 4b is barely discernable, indicating a lower dissociation fraction for 355-nm one-photon ionization; and (4) the total signal $R^+ + P^+$ in Figure 4b is an increasing function, indicating that $i_b > i_a$ [eq 3]. The data in Figure 4 are fitted to eqs 1 and 2 assuming $i_b/i_a = 2.0$ and $f_a = 0$ and yield values of $f_b = 0.96$ (for λ_2 = 532 nm) and $f_b = 0.65$ (for λ_2 = 355 nm). Because the absolute intensity scale was not accurately recorded, the fitting of $R^+(t)$ and $P^+(t)$ was done without benefit of eq 3, which would have provided a better estimate of the relative ionization cross sections.

Calculated traces are presented in Figure 6 to show how the time-dependent yields of reactant and product ion vary with changes in the relative ionization cross section i_b/i_a and the outer well dissociation fraction f_b. For these calculations we assume that inner well dissociation is negligible (i.e., $f_a = 0$). The effect of $f_a > 0$ is to add a step function response to the time-dependent product signal $P^+(t)$; the shape of the $R^+(t)$ curve remains unchanged. For the ideal limiting case where $f_a = 0$ and $f_b = 1$, one obtains the simple set of equations $R^+(t) = R_0^* i_a \exp\{-kt\}$ and $P^+(t) = R_0^* i_b(1 - \exp\{-kt\})$.

5. Electronic Basis for Proton Transfer in Cluster Ions

Gas-phase ion–molecule studies have provided evidence that an activation barrier and double-minima reaction coordinate exist for certain classes of proton transfer reactions.[27,28,33,34] In a

(31) Although a single 532-nm photon exceeds the measured vertical E_{IP} for the larger $PhOH(NH_3)_n$ clusters [e.g., $E_{IP}(n = 4)$ = 6.89 eV versus $h(\nu_1 + \nu_2)$ = 6.99 eV for 266 + 532 nm REMPI], the ionization efficiencies at threshold are very small (ref 8).

(32) Lias, S. G.; Liebman, J. F.; Levin, R. D. *J. Phys. Chem. Ref. Data* **1984**, *13*, 695.
(33) Meot-Ner, M. *J. Am. Chem. Soc.* **1982**, *104*, 5.
(34) Bass, L. M.; Cates, R. D.; Jarrold, M. F.; Kirchner, N. J.; Bowers, M. T. *J. Am. Chem. Soc.* **1983**, *105*, 7024.

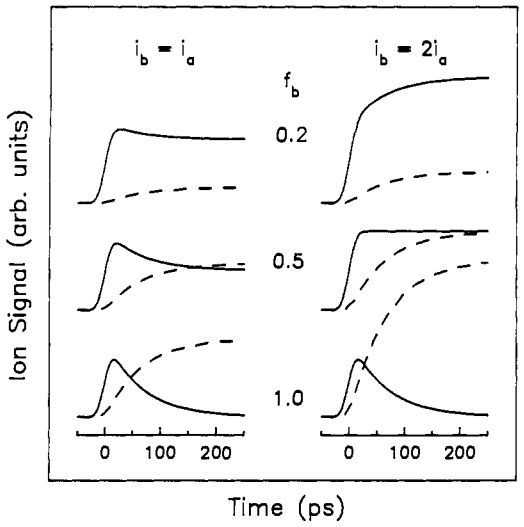

Figure 6. Calculated reactant $R^+(t)$ [eq 1, (–)] and product ion $P^+(t)$ [eq 2, (– – –)] time-dependence as a function of inner and outer well ionization cross sections (i_a and i_b) and dissociation fractions (f_a and f_b). Calculations assume $f_a = 1$ and $1/k = 65$ ps.

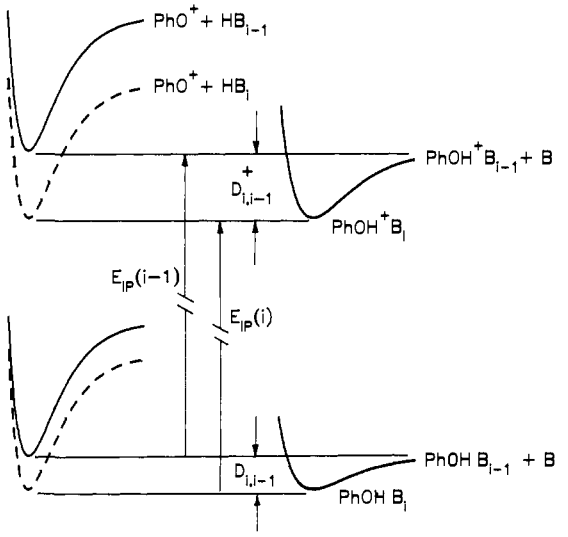

Figure 7. Definition of terms for stepwise solvation energies $D^+_{i,i-1}$ and $D_{i,i-1}$ for phenol cation and neutral, respectively, and measurable ionization potentials E_{IP}.

number of cases, rather slow reaction rates were measured for very exothermic reactions,[27] which was explained by a barrier process attributed to steric hindrance or charge delocalization. It seems plausible that charge delocalization creates a barrier to proton transfer because the transfer of charge must go by an electronic transition or a curve crossing. In this section we use simple chemical notions to support this viewpoint and show how the addition of solvent molecules modifies the reaction coordinate.

Definition of Solvation Energies. We define in Figure 7 the stepwise solvent binding energies for neutral ($D_{i,i-1}$) and cationic ($D^+_{i,i-1}$) phenol in their ground electronic states. (The subscript $i,i-1$ refers to an increase in solvent size from $i-1$ to i.) These data are related to changes in the ionization energy E_{IP}[35-38] by the relation

$$\Delta E^{IP}_{i,i-1} = E_{IP}(i-1) - E_{IP}(i) = D^+_{i,i-1} - D_{i,i-1} \quad (4)$$

The value of $D^+_{i,i-1}$ derives from charge–dipole and charge-induced–dipole interactions and is typically a much stronger interaction than $D_{i,i-1}$, which arises from hydrogen-bonding electrostatic attraction between neutral molecules. As i increases, the charge becomes increasingly shielded in the growing cluster ion, and $D^+_{i,i-1}$ approaches $D_{i,i-1}$ in value.

We define the sequential proton solvation binding energies as follows

$$H^+B_{i-1} + B \rightarrow H^+B_i \qquad \Delta H = D^{H^+}_{i,i-1}$$

These values have been measured from high-pressure flow-tube equilibrium studies.[1] One should note that the total solvation energy given by

$$H^+ + nB \rightarrow H^+B_n \qquad \Delta H = \sum_{i=1}^{n} D^{H^+}_{i,i-1}$$

is related to, but not the same as, the cluster proton affinity, which is defined as

$$H^+ + B_n \rightarrow H^+B_n \qquad \Delta H = D(H^+ - B_n)$$

When written as a thermodynamic cycle, it follows that the total solvation energy is greater than the cluster proton affinity by the sum of the neutral solvent–solvent binding energies $\sum D_{i,i-1}$ (i.e., the energy for $nB \rightarrow B_n$). A compilation of NH_3 solvation energies is given in Table I.

Potential Energy Curves. We begin by constructing potential curves for the isolated phenol cation and then determining single-molecule stabilization energies at fixed positions along the potential curves (e.g., at the minima and dissociative limits). The energies at the well depths and the dissociative limits for the phenol cation are determined as follows: The minimum energy for the ground-state ion is assumed to be equivalent to the ionization potential of phenol ($E_{IP} = 8.51$ eV[36b]). The cation dissociation energy $D(PhO^+H)$ was determined from the thermodynamic cycle

$$PhOH^+ + e^- \rightarrow PhOH \qquad -E_{IP}(PhOH)$$
$$PhOH \rightarrow PhO + H \qquad D(PhOH)$$
$$PhO \rightarrow PhO^+ + e^- \qquad E_{IP}(PhO)$$

where it follows that

$$D(PhO^+H) = E_{IP}(PhO) - E_{IP}(PhOH) + D(PhOH)$$
$$= 8.56 - 8.51 + 3.75 = 3.80 \text{ eV}$$

(the reported values are from refs 39, 36b, and 40). About 70% of the positive charge in the ground-state ion is confined to the aromatic ring,[41] which may explain why the O–H dissociation energy is similar to that in the neutral ground state molecule. We therefore assume that the O–H bond is covalent and can be described by a Morse potential of the form

$$V(r) = D\{1 - \exp[-\beta(r - r_e)]\}^2 \quad (5)$$

We assume an equilibrium O–H bond length of $r_e = 0.95$ Å,[42] and a vibrational amplitude for an O–H fundamental of 0.16 Å.[43] The five lowest lying electronic states (<13 eV) are calculated to have aromatic ring charge ranging from 45%–100%.[41] We show only the n-orbital open-shell state at about 3 eV[41,44] corresponding to 45% ring charge. These intermediate excited-state Morse-type

(35) (a) Lipert, R. J.; Colson, S. D. *J. Phys. Chem.* **1990**, *94*, 2358. (b) Lipert, R. J.; Colson, S. D. *J. Chem. Phys.* **1988**, *89*, 4579. (c) Lipert, R. J.; Bermudez, G.; Colson, S. D. *J. Phys. Chem.* **1988**, *92*, 3801.

(36) (a) Fuke, K.; Kaya, K. *Chem. Phys. Lett.* **1983**, *94*, 97. (b) Mikami, N.; Suzuki, I.; Okabe, A. *J. Phys. Chem.* **1987**, *91*, 5242.

(37) (a) Hagar, J.; Wallace, S. C. *J. Phys. Chem.* **1985**, *89*, 3833. (b) Hagar, J.; Leach, G. W.; Demmer, D. R.; Wallace, S. C. *J. Phys. Chem.* **1987**, *91*, 3750.

(38) The measurement of E_{IP} values by photoionization involves vertical transitions, which can overestimate the adiabatic value.

(39) Lias, S. G.; Bartmess, J. E.; Liebman, J. F.; Holmes, J. L.; Levin, R. D.; Mallard, W. G. *J. Phys. Chem. Ref. Data* **1988**, *17*, 1.

(40) McMillen, D. F.; Golden, D. M. *Ann. Rev. Phys. Chem.* **1982**, *33*, 493, and references therein.

(41) Rabalais, J. W. *Principles of Ultraviolet Photoelectron Spectroscopy*; Wiley: New York, 1977; p 301ff.

(42) Pimentel, G. C.; McClellan, A. L. *The Hydrogen Bond*; W. H. Freeman: San Francisco, CA, 1960.

(43) The vibrational amplitude is calculated from the classical turning points of a harmonic oscillator and is defined from the equilibrium position to the classical turning point. We use a fundamental frequency of 3500 cm^{-1} for PhOH.

(44) van Velzen, P. N. T.; van der Hart, W. J.; van der Greet, J.; Nibbering, N. M. M.; Gross, M. L. *J. Am. Chem. Soc.* **1982**, *104*, 1208.

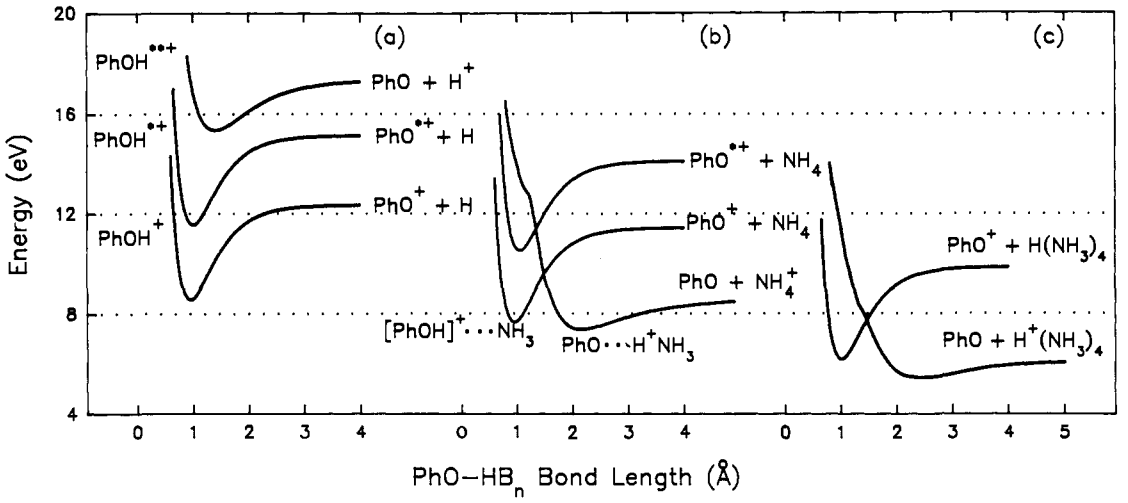

Figure 8. Approximate $[PhOH]^+(NH_3)_n$ cluster ion potential energy curves for the reactive PhOH coordinate: (a) $n = 0$, (b), $n = 1$, and (c) $n = 4$. Energies are relative to the unsolvated $PhOH^+$ cation.

curves, which correlate with neutral H atom dissociation, are not directly involved in proton transfer.

The highest energy curve in Figure 8a is very important because it correlates with the acid dissociation PhO + H^+. The asymptotic energy relative to the ground-state curve is determined from the following thermodynamic cycle (written in a shorthand notation):

$$PhOH^+ \xrightarrow{3.80} PhO^+ + H \xrightarrow{13.60}$$

$$PhO^+ + H^+ + e^- \xrightarrow{-8.56} PhO + H^+ \qquad \Delta H = 8.84 \text{ eV}$$

This value is equivalent to the proton affinity of PhO and agrees with a reported value of 8.8 eV.[32] We do not know what excited electronic state correlates with the PhO + H^+ dissociation except to guess that it must have positive charge localized near to or on the H atom. We assume that the PhO + H^+ bond for this higher excited state $[PhOH^{**}]^+$ is more like an ion-induced–dipole interaction than a covalent interaction, in which case the bound potential is extended and shallow (~1.5 Å bond length and ~2 eV well depth). The details of the well region are actually not that important as far as solvation dynamics are concerned, as we shall see shortly.

The potential curves for the cluster ions are modified relative to the isolated molecule on the basis of a simple principle. Regions of the potential curve that have large proton character (e.g., the PhO + H^+ dissociative limit) are stabilized enormously by the proton affinity of the solvent, whereas those regions with little proton character (e.g., in the case of large aromatic charge density) are stabilized by the solvent to a much lesser extent. The potential curves for singly solvated phenol cation in Figure 8b were constructed as follows: The reduction in energy of the $[PhOH]^+$ ground-state potential is obtained from ionization threshold measurements for stepwise solvation [eq 4 and Table I].[8,35-38] The solvent–cation bond energy for a single NH_3 molecule is about 0.87 eV. The O–H bond energy for the cation ground state is probably only slightly weakened due to solvation since the charge stabilization is confined mostly to the aromatic ring; hence, we shift the potential curve uniformly by 0.87 eV. The lower excited ion states also have large aromatic charge density[41] and are, therefore, assumed to have a covalent O–H bond that is not affected much by solvation. We estimate a stabilization of this excited state by a single solvent molecule of 1 eV.[45,46]

The uppermost curve shown in Figure 8a is strongly affected by base solvent because the PhO + H^+ asymptote is stabilized by the proton affinity of the solvent cluster (Table I). Although we have no information on the properties of $[PhOH^{**}]^+$, we would guess that the solvent stabilization of this state is much less than that for H^+; hence, the potential curve becomes repulsive upon solvation. This repulsive curve crosses the ground-state curve and develops a shallow well at an extended bond distance due to hydrogen bonding (or ion–dipole interaction) between PhO and H^+. The bond energy can be estimated as follows. The proton affinity of PhO and NH_3 are reported to be about the same.[32,47] Hence, we expect that the bond energy for PhO···H^+NH_3 should be similar to that for H_3N···H^+NH_3. The latter energy is 1.08 eV (Table I). We assume a bond length of about 2.0 Å based on the calculated bond length of 1.8 Å for the stronger PhO^-···H^+NH_3 ion pair. For comparison, we note that the calculated bond length for H_2O···H^+NH_3 is 1.74 Å.[48]

The changes in the potential energy curves induced by additional solvent molecules are estimated with the thermodynamic data in Table I for stepwise binding energies. A tabulation of energies for the reactant, complex, and product structures is given in Table II (the values in columns II, IV, and V pertain to Figure 8). The curves for phenol cation clustered to four NH_3 solvent molecules are given in Figure 8c. The potential energy curves are consistent with the observed chemistry of $PhOH^+$ in solvent clusters, namely (1) a large barrier to reaction from an inner well, (2) a weakly bound outer potential well that is reduced in energy by base solvent

Table I. Stepwise Solvation Energies (eV) for the Reaction $M^+(NH_3)_{i-1} + NH_3 \rightarrow M^+(NH_3)_i$

	M = PhOH			M = H[a]	
i, n	$\Delta E^{IP}_{i,i-1}$[b]	$D^+_{i,i-1}$[c]	$\sum_{i=1}^{n} D^+_{i,i-1}$	$D^{H^+}_{i,i-1}$	$\sum_{i=1}^{n} D^{H^+}_{i,i-1}$
1	0.65	0.87[d]	0.87	8.84	8.84[e]
2	0.16	0.36	1.23	1.08	9.92
3	0.16	0.34	1.57	0.76	10.68
4	0.62	0.79	2.36	0.60	11.28
5	0.00	0.16	2.52	0.54	11.82
6				0.33	12.15
10[f]		0.15		0.15	

[a] Solvation energies from ref 1, unless otherwise noted. [b] Reference 8. [c] Calculated from eq 4 and assuming $D_{i,i-1}$ values ranging from 0.22 eV ($i = 1$) (ref 29) to the large i limit, which we equate to the reported NH_3–NH_3 dimer bond energy of 0.15 eV (ref 55). [d] Mikami reports this value to be 1.01 eV based on an E_{IP} of 7.71 eV (ref 29). We use E_{IP} = 7.85 eV (ref 8), which leads to a value of $D^+_{i,i-1}$ = 0.87 eV. [e] Reference 32. [f] $n = 10$ is assumed to approximate the bulk phase for which we have assigned neutral–neutral binding energies (cf. footnote *c*).

(45) The solvent stabilization of the aromatic charge, however, is expected to be somewhat larger than in the ground-state ion in analogy with measured solvent stabilization energies of neutral electronic states (refs 35, 36, and 46).

(46) (a) Gonohe, N.; Abe, H.; Mikami, N.; Ito, M. *J. Phys. Chem.* **1985**, *89*, 3642. (b) Oikawa, A.; Abe, H.; Mikami, N.; Ito, M. *J. Phys. Chem.* **1983**, *87*, 5083.

(47) Actually, PhO must have a lower proton affinity than NH_3 to account for the greater yield of DPT versus evaporation.

(48) Deakyne, C. A. *J. Phys. Chem.* **1986**, *90*, 6625.

Table II. Cluster Size Dependent Energies (eV) Relative to $[PhOH]^+ + n(NH_3)$[a,b]

n	I[c] $[PhOH]^+ + B_n$	II[d] $[PhOH]^+B_n$	III $[PhO\cdots H^+\cdots B_n]^{2+}$	IV $PhO{\cdot}H^+B_n$	V[e] $PhO + H^+B_n$
0	0	0		~5-7	8.82
1	0.00	-0.87	*0.6*	-1.08	-0.02
2	-0.15	-1.23	*-0.1*	-1.84	-1.10
3	-0.30	-1.57	*-0.8*	-2.44	-1.86
4	-0.45	-2.36	*-1.8*	-2.98	-2.46
5	-0.60	-2.52		-3.31	-3.00
6	-0.75				-3.33
10[f]	-1.35	*-3.57*	*-3.2*	*-4.52*	*-4.39*

[a] $[PhOH]^+ + n(NH_3)$ is at 8.51 eV relative to PhOH + $n(NH_3)$ (ref 36b); $n(NH_3)$ refers to uncomplexed, isolated NH_3 molecules. [b] Values in italics are reported with less confidence than the other values. [c] Based on NH_3–NH_3 dimer bond energy of 0.15 eV (ref 55). [d] The values in this column are obtained from Table I, column III. [e] The B_n cluster proton affinity (PA) can be determined from the relation $PA_n = 8.82 - (V - I)$, where 8.82 eV is the PA of PhO (ref 32) and I and V are column designations. [f] These values were computed by extrapolating asymptotically to the bulk-phase limit.

Table III. Phenol–Solvent Energy Data (eV) Pertinent to DPT Reaction

B	ΔH_g	$\Delta E^{IP}_{1,0}$	$D_{1,0}$	$D^+_{1,0}$	$D^{H^+}_{2,1}(H^+B{-}B)$	$D^{PA}_{1,0}(H^+{-}B)$[a]	$\Delta H_{s,1}$
H_2O	1.46	0.57[b]	0.20[g]	0.77	1.46	7.36	2.23
CH_3OH	0.92	0.65[c]	0.20[g]	0.85		7.90	1.77
NH_3	-0.01	0.65[d]	0.22[h]	0.87	1.08	8.84	0.86
$N(CH_3)_3$	-0.94	1.51[e]	0.56[e]	2.07[e]		9.76	1.13
		(0.81)[f]		(1.37)[f]			(0.43)[f]

[a] Reference 32. [b] Reference 46b. [c] Reference 35. [d] Reference 8. [e] Mikami et al. (ref 56). [f] Because E_{IP} = 7.81 eV for TMA and 8.51 eV for phenol, we believe that the first ionization threshold measured by Mikami et al. (ref 56) at 7.0 eV is due to $PhOH^*(TMA)^+$ and that the second threshold at 7.7 eV is due to $PhOH^{+*}(TMA)$. We favor the values in parentheses which assume 7.7 eV as the relevant solvated phenol ionization threshold. [g] Estimated based on typical hydrogen bond energies (refs 42 and 52). [h] Mikami et al. (ref 29).

molecules to a much greater extent than the inner well, and (3) a reaction enthalpy that is exothermic for NH_3 cluster sizes of $n > 2$.

Enthalpies and Activation Energies. We define the reaction enthalpy for cluster ion DPT as the difference in energy between the minima of the inner potential well and the dissociative limit of the outer well. (These values are listed in Table II.) It is instructive to begin with the bimolecular gas-phase reaction

$$[PhOH]^+ + B \rightarrow PhO + H^+B$$

where B is the solvent molecule. A thermodynamic cycle can be written leading to the gas-phase reaction enthalpy

$$\Delta H_g = E_{IP}(H) - E_{IP}(PhOH) + D(PhO{-}H) - D(H^+{-}B) \quad (6)$$

$$= 13.60 - 8.51 + 3.73 - 8.84 = -0.02 \text{ eV}$$

(where the data have been referenced earlier). The singly solvated cluster reaction differs from the gas-phase reaction in that the reactant side is stabilized by the hydrogen bond energy $[PhOH]^+\cdots B$. The solvent stabilized enthalpy $\Delta H_{s,n}$ for a single solvent molecule is then given by

$$\Delta H_{s,1} = \Delta H_g + D^+_{1,0}([AH]^+ - B) \quad (7)$$

$$= -0.02 + 0.87 = 0.85 \text{ eV}$$

where the binding energies $D^+_{i,i-1}$ (defined in Figure 7) are listed in Table I. Single solvation has the curious effect of raising rather than lowering the reaction enthalpy.[9b,49] This occurs because only the reactant side is stabilized by the solvent bond. However, for larger cluster sizes, the additional solvent molecules bond to both reactant and product. Because base solvent molecules, such as NH_3, form stronger bonds to the protonated product ion than to the unprotonated reactant ion, there is a cumulative lowering of the enthalpy with increasing solvent size. The enthalpy for the solvated cluster dissociation

$$[PhOH]^+B_n \rightarrow PhO + H^+B_n$$

depends on the additive stepwise solvation energies of both reactant and product ion according to the equation

$$\Delta H_{s,n} = \Delta H_g + \sum_{i=1}^{n} D^+_{i,i-1} - \sum_{i=2}^{n} D^{H^+}_{i,i-1} \quad (8)$$

The second summation begins at $i = 2$ because the $i = 1$ term is already incorporated as the proton affinity $D(H^+{-}B)$ in eq 6. The value of $\Delta H_{s,n}$ can also be obtained by subtracting the values in column V from column II in Table II.

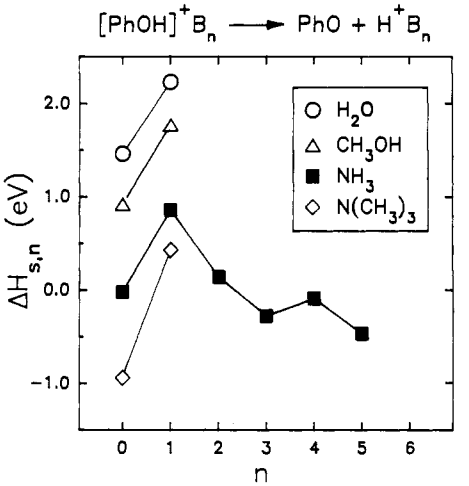

Figure 9. Enthalpies for stepwise solvation of DPT in $[PhOH]^+B_n$ clusters. The first point for each solvent B corresponds to the bimolecular gas-phase reactants $[PhOH]^+ + B$.

Computed values of $\Delta H_{s,n}$ are plotted in Figure 9. Results for solvents other than NH_3 are limited because of the lack of $\Delta E^{IP}_{i,i-1}$ measurements, which are needed to compute $D^+_{i,i-1}$ values [eq 4]. We include only single-solvation cluster enthalpies based on the reported data in Table III. The general ordering of solvent cluster basicity for small clusters is dominated by the gas-phase proton affinity (with B = H_2O being the least basic). For B = NH_3, the gas-phase bimolecular reaction is approximately thermoneutral due to the similar proton affinity for PhO and NH_3.[32,47] The solvated reaction is calculated to become exothermic at $n > 2$. We note that the free energy $\Delta G = \Delta H - T\Delta S$ will be less than ΔH due to the positive value of ΔS for DPT. However, we do not know the magnitude of ΔS, nor the cluster ion temperatures. Because T is likely to be small, it is probably safe to assume that $\Delta H \sim \Delta G$ to within 0.2 eV.

The experimental results in Figures 2–5 indicate that the $[PhOH]^+(NH_3)_n$ cluster ions are significantly less reactive from the inner potential well than from the outer well. These obser-

vations are in accord with our model of an energy barrier that impedes the exothermic dissociation. We are not aware of any reported work concerning activation energies of proton-transfer reactions in clusters (in fact very little is known for the more extensively studied topic of gas-phase ion–molecule reactions[21-23,27,28,33,34]). It therefore seemed worthwhile to provide at least some rough estimates of cluster size-specific activation energies, $E_{0,n}$, based on our simple picture of the potential energy curves in Figure 8. By equating $E_{0,n}$ to the energy at the diabatic curve crossing, we obtain upper limits ranging from 1.5 (n = 1) to 1.0 eV (n = 4). We have ignored vibrationless energies and the magnitude of the splitting at the avoided crossing; both effects could reduce the value of $E_{0,n}$ by upwards of 0.5 eV. The gas-phase bimolecular energy barrier relative to the separated reactant molecules is about 0.6 eV. These values have large uncertainties (perhaps as much as one eV) due to serious difficulties in defining the crossing region that defines the barrier height (i.e., not knowing the precise shape of the potential curves, the vibrational amplitudes, or the magnitude of the splitting). Still, these rather crude estimates of $E_{0,n}$ are instructive for understanding relative trends in the progressive solvation of a chemical reaction.

The maximum energy available to a particular cluster ion is given by the difference between the photon energy (9.32 eV for 1-C 266-nm REMPI) and the cluster E_{IP} energies; these differences being 1.5 (n = 1), 1.6 (n = 2), 1.8 (n = 3), and 2.4 eV (n = 4). Compared to the crude estimates of $E_{0,n}$, sufficient excitation energy is available for inner well DPT at $n \geq 2$ for 266-nm ionization and at $n \geq 4$ for 355-nm ionization. That neither ionization energy leads to DPT indicates that either the values of $E_{0,n}$ are larger than estimated or that the distribution of ion vibrational energies is much less than the excess photon energies (quite likely depending on the Franck–Condon factors). Mikami et al. reported that the dimer $PhOH^+\cdots NH_3$ fails to undergo DPT at ionization energies exceeding 1 eV above the ion minimum, yet the nearly equienergetic dissociation to form $PhOH^+ + NH_3$ occurs readily at these energies.[29] This result is consistent with our conclusion that a substantial barrier exists to DPT from the inner potential well. There is no evidence of barrier tunneling, which is common for proton-transfer reactions involving small barriers in solution.[50] Presumably, the strong solvent cation bond causes the solvent to move with the proton. This increase in reduced mass would preclude the possibility of tunneling. Finally, we mention that we are only sensitive to reactions that occur within our mass spectrometer response time of about 1 μs; slower reactions would go undetected.

6. Bimolecular Reactive Surface—Relation to Bulk Phase

Bimolecular collisions can produce the same reactive complexes associated with clusters and solution phase, except that they occur at higher energy because of the energy gained through the attractive force of the reactants. We recast the double well cluster potentials, which represent minimum energy paths, to 2D reactive potential energy surfaces[51] in order to explicitly include the bond-making coordinate $[PhOH]^+\cdots B_n$ and the bond-breaking coordinate $PhO\cdots H^+B_n$. We use the minima energies, barrier heights, and dissociative energies, compiled in Table II, and assume Morse-type potentials. The bond distances at the minima positions are based on the best available information,[48,52-54] and the widths of the wells are determined from estimated vibrational amplitudes.[43] We also include the energy for the $PhO + H^+ + B_n$ dissociation limit. These data were reduced to a 10 × 10 grid, and a contour surface was fitted to the points with a spline-fitting and interpolation routine from a 3D contour drawing program. The accuracy of the surface is estimated to be about ±0.25 eV for the regions shown (i.e, part of the repulsive wall, well-depths, barriers, and dissociative limits). The extremities of the repulsive wall are less certain and not shown. The interpolation routine

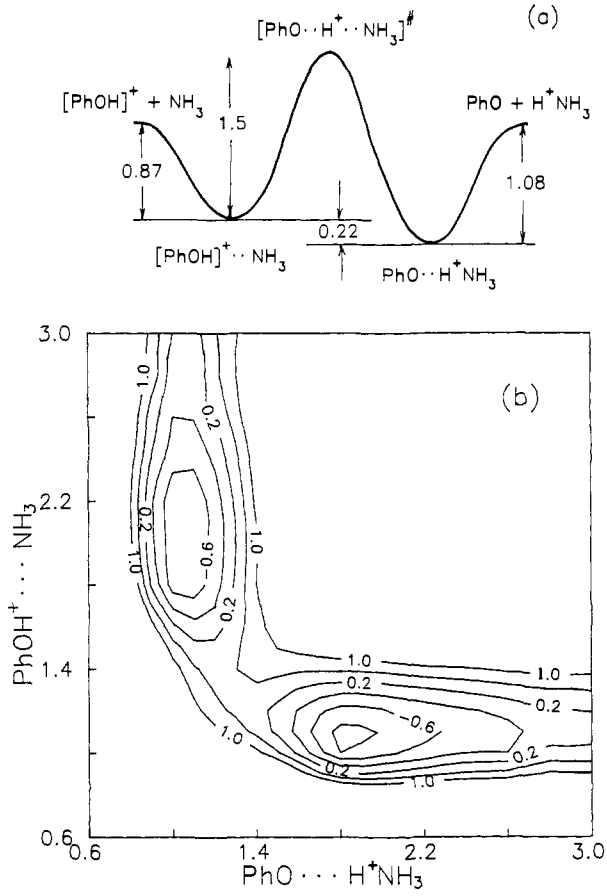

Figure 10. Reactive potential energy surface for $[PhOH]^+ + NH_3$: (a) minimum-energy reaction coordinate and (b) 2D collinear potential energy surface. Energies (eV) are relative to reactant asymptotic limit. Contour spacings are 0.4 eV.

introduces some distortions at the edges. The overall accuracy is sufficient for this discussion. We choose the collinear O···H···N geometry because this corresponds to the most stable hydrogen bond configuration.

The 2D potential surfaces in Figures 10 and 11 describe three classes of reaction. Bimolecular gas-phase reactions are represented by the path from dissociative limit to dissociative limit

$$[PhOH]^+ + B_n \rightarrow PhO + H^+B_n \qquad \Delta H_{bc}$$

Cluster-phase DPT, which is a bimolecular half-collision, corresponds to a path from the first minimum to the dissociative limit

$$[PhOH]^+B_n \rightarrow PhO + H^+B_n \qquad \Delta H_{s,n}$$

and has been treated in detail in the previous section. Solution-phase acid–base chemistry is represented by the path from one minimum to the other minimum

$$[PhOH]^+B_n \rightarrow PhO{\cdot}H^+B_n \qquad \Delta H_{soln}$$

Each type of reaction shares the same transition state. The 2D surface is certainly not complete because it does not consider all the solvent coordinates that would, for example, prevent $PhOH^+$ in bulk solvent from separating from the solution. This resistance is, however, partially accounted for by the solvation energies which deepen the entrance channels with increasing n (compare Figures 10 and 11). However, this trend only continues for a few solvation shells, beyond which the solvation energy difference, $D^+_{i,i-1} + D_{i,i-1}$, approaches zero.

The reaction enthalpies for bimolecular collisions (ΔH_{bc}), solvated clusters (ΔH_s), and (micro-) solution phase (ΔH_{soln}) are plotted in Figure 12 along with the activation energy $E_{0,n}$, which is common to all three classes of reactions. ΔH_{bc} is the most exothermic because it corresponds to separated reactant species which lie at higher energy than the bound reactants (Figures 10a

(49) (a) Garvey, J. F.; Bernstein, R. B. *J. Am. Chem. Soc.* **1987**, *109*, 1921. (b) Bohme, D. K.; Rakshit, A. B.; Mackay, G. I. *J. Am. Chem. Soc.* **1982**, *104*, 1100.

(50) Rentzepis, R. M.; Barbara, P. F. *Adv. Chem. Phys.* **1981**, *47*, 627.

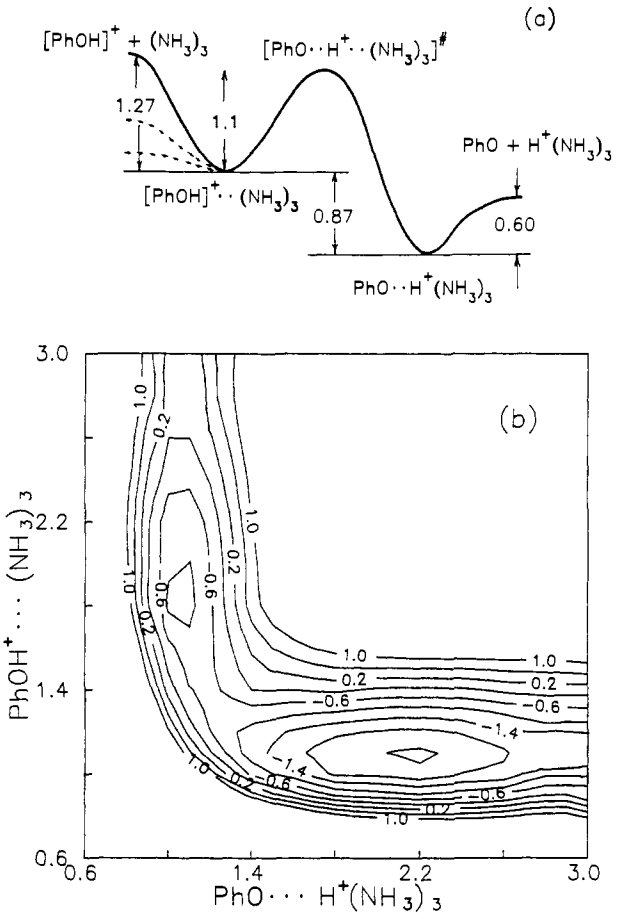

Figure 11. Reactive potential energy surface for $[PhOH]^+ + (NH_3)_3$. (a) Minimum-energy reaction coordinate: The dashed line on the reactant side denotes $PhOH^+NH_3 + (NH_3)_2$ and $PhOH^+(NH_3)_2 + NH_3$, respectively. (b) 2D collinear potential energy surface: Energies (eV) are relative to reactant asymptotic limit. Contour spacings are 0.4 eV.

and 11a). Not shown in Figure 12 are the hypothetical series of bimolecular collisions represented by

$$[PhOH]^+B_{n-m} + B_m \rightarrow PhO + H^+B_n$$

whose enthalpies span the range from pure bimolecular ($m = n$, ΔH_{bc}) to cluster half-collision dissociation ($m = 0$, ΔH_s). This direct connection between the energetics of bimolecular and cluster reactions is illustrated in Figure 11a.

Perhaps the more interesting correspondence is that between cluster reactions and solution-phase chemistry. The reaction enthalpies for these two cases clearly converge for increasing n (Figure 12). The enthalpy difference starts out large for small n because of the strong charge–dipole attraction involving PhO and H^+B_n, which must be overcome to form products. As n increases and the charge becomes delocalized by the solvent, this interaction diminishes and the difference between ΔH_s and ΔH_{soln} reduces to a weak neutral solvent hydrogen bond energy, which is about 0.15 eV for NH_3.[52,55] This asymptotic energy difference at large n arises because we defined the cluster reaction to involve a dissociation in order to produce a detectable product H^+B_n.

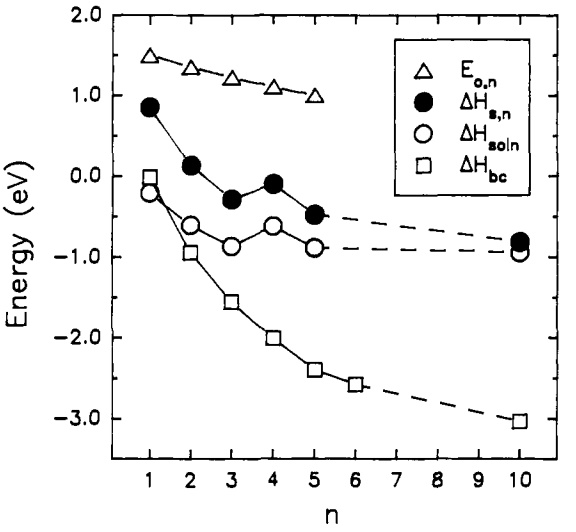

Figure 12. Reaction enthalpies for bimolecular, cluster, and solution-phase proton transfer. Activation energies are measured from the classical well depth of the first minimum structure $[PhOH]^{*+}(NH_3)_n$ to the diabatic crossing point.

Large-size cluster reactions, in fact, converge exactly to solution phase if we define the bound complex $PhO^*H^+B_n$ as the product.

Finally, we comment on the activation energy $E_{0,n}$. Because the bimolecular, cluster, and solution-phase reactions involve the $[PhOH]^+B_n$ complex, they are all influenced by $E_{0,n}$. This is a real barrier for the latter two reactions because they exist at the minimum position. The barrier is also important for bimolecular collisions, even when the reactant energy exceeds $E_{0,n}$. The barrier along the reaction coordinate merely represents the minimum energy path to product. The 2D coordinate potential energy surfaces in Figures 10 and 11 begin to show the multidimensional scale of the problem. In these 2D cuts of the reactive hypersurface (involving all internal modes of the complex), the barrier height is a saddle point, with energy rising steeply in directions orthogonal to the minimum energy path. Sufficient reactant energy must be directed along the reaction coordinate (i.e., reactive mode), otherwise the trajectory will bounce around (vibrate) in the entrance channel and reflect back out as reactants. An exchange of reactant internal energy will occur (inelastic collision), but no reaction will take place.

7. Conclusions

The dissociative proton transfer (DPT) reaction involving the aromatic acid phenol cation was studied as a function of single-molecule sequential solvation in molecular clusters of NH_3, CH_3OH, H_2O, and the other hydrogen-bonding solvents. The use of molecular clusters for studying chemical reactions provides a very important and new perspective to understanding solvation effects. The unique contribution of this work is based on our ability to produce cluster ions at different positions along a reactive potential energy surface by using delayed picosecond ionization from an intermediate reactive state. This capability has allowed us to elucidate the shape of the reactive potential energy surface for progressive solvation. We have shown that acid–base chemistry of aromatic cations in small solvent shells proceeds along a double minima potential curve separated by a large barrier. This feature is expected to be a general property of ionic acids that have charge delocalized from the departing proton. It is also worth noting that the use of delayed picosecond ionization is a method that can be exploited to produce either of the two isomeric cluster ion forms in rather high purity.

Molecular clusters represent a state of matter that is intermediate between the gas phase and condensed phase. A large part of this paper is concerned with establishing a framework for relating these two limits of conventional chemistry. The chemical properties of clusters as a function of cluster size provides the essential link. On the basis of our experimental results together with literature data, we have constructed detailed potential energy

(51) Levine, R. D.; Bernstein, R. B. *Molecular Reaction Dynamics and Chemical Reactivity*; Oxford University Press: New York, 1987.
(52) (a) Dykstra, C. E. *J. Phys. Chem.* **1990**, *94*, 6948. (b) Nelson, D. D., Jr.; Fraser, G. T.; Klemperer, W. *Science* **1987**, *238*, 1670.
(53) Welti, M.; Ha, T.-K.; Pretsch, E. *J. Chem. Phys.* **1988**, *83*, 2959.
(54) (a) Herbine, P.; Dyke, T. R. *J. Chem. Phys.* **1985**, *83*, 3768. (b) Damewood, J. R., Jr.; Kumpf, R. A.; Mühlbauer, W. C. F.; Urban, J. I.; Eksterowicz, J. E. *J. Phys. Chem.* **1990**, *94*, 6619.
(55) (a) Ceyer, S. T.; Tiedemann, P. W.; Mahan, B. H.; Lee, Y. T. *J. Chem. Phys.* **1979**, *70*, 14. (b) Greer, J. C.; Ahlrichs, R.; Hertel, I. V. *Chem. Phys.* **1989**, *133*, 191.
(56) Mikami, N.; Suzuki, I.; Okabe, A. *J. Phys. Chem.* **1987**, *91*, 5242.

curves for conditions ranging from the isolated gas phase to the bulk-solvated limit. We have also presented a picture of the evolution of gas-phase to condensed-phase chemistry from the viewpoint of bimolecular reactive scattering, reducing the problem to the most relevant reactant and solvent coordinates. Although large polyatomic ion–molecule collisions and cluster reactions are not amenable to quantal or even classical trajectory calculations for large regions of hyperspace, progress may be possible by reducing the problem to a few essential degrees of freedom. In this spirit we have derived empirical 2D potential energy surfaces for representative cluster sizes.

Acknowledgment. This work was supported by the Aerospace Sponsored Research program.

Registry No. $PhOH^+$, 40932-22-7; NH_3, 7664-41-7; H_2O, 7732-18-5; CH_3OH, 67-56-1; NMe_3, 75-50-3.

Observation of the Doubly Charged, Gas-Phase Fullerene Anions C_{60}^{2-} and C_{70}^{2-}

Patrick A. Limbach, Lutz Schweikhard,† Kenneth A. Cowen, Mark T. McDermott, Alan G. Marshall,*,‡ and James V. Coe*

Contribution from the Department of Chemistry, 120 West 18th Avenue, The Ohio State University, Columbus, Ohio 43210. *Received April 2, 1991*

Abstract: The fullerenes exhibit a remarkable ability to accommodate excess negative charge. We have observed C_{60}^{2-} and C_{70}^{2-} in a Fourier transform ion cyclotron resonance mass spectrometer by laser desorption (1.064 μm) of raw fullerene material that had been extracted from soot produced from graphite rods. C_{60}^{2-} was distinguished from C_{30}^{-} by the relative abundances and m/z values of its isotopic ions. C_{60}^{2-} was distinguished from the double harmonic of C_{60}^{-} by selective ejection of C_{60}^{-}, selective excitation of C_{60}^{2-}, and by a new and definitive method based upon comparing frequency shifts of singly and doubly charged ions as a function of ICR trapping voltage.

Introduction

The advent of techniques for producing gram quantities of the new form of pure, solid carbon[1,2] (buckminsterfullerene) has made feasible a wide range of new experiments drawn from a variety of scientific disciplines. One notable property of the fullerenes is an unusual ability to accomodate negative charge. On the basis of ab initio calculations,[3] Pitzer and co-workers have suggested that C_{60}^{2-} may be stable in the gas phase. In solution, multiple electrons have been readily added to C_{60} by means of cyclic voltammetry.[4,5] The present investigation focuses on experimental demonstration of the existence of the doubly charged fullerence anions in the gas phase.

Reports of doubly charged, gas-phase anions are fairly rare,[6-10] even though chemists frequently encounter such species in the condensed phases of matter. One strategy for accommodating two like charges is to separate them by as much distance as possible within the molecule, as is illustrated by certain doubly charged gas-phase sulfonates[6] and carboxylates.[7] Another strategy involves the production of gas-phase cluster ions that mimic the solvation of ions in the liquid phase. Solvation provides the stabilization for many familiar doubly charged negative ions that have never been seen in the gas phase as monomers, such as SO_4^{2-}. Clusters also provide opportunities for charge delocalization among equivalent sites. Double negative charges have been reported for oxygen cluster ions.[8] A few small polyatomics may be so electronegative that they can accommodate more than one excess electron, such as NO_2^{2-},[9] and perhaps AuF_6^{3-}.[10] Although there have been reports of doubly charged atomic negative ions, those reports have since been disputed.[6,11,12]

Buckminsterfullerene consists of 60 carbon atoms that assume the shape of a soccer ball. It is aromatic and has icosahedral symmetry, the highest possible symmetry for any molecule. The existence of this molecule was first inferred from laser vaporization studies of carbon clusters by Smalley and co-workers.[13,14] A crucial practical breakthrough occurred when Huffman and co-workers[15] demonstrated that fullerenes could be produced in abundance by evaporating graphite electrodes. Improvements in their technique[16] and an alternative carbon arc technique[17] have

† Ohio State University Postdoctoral Fellow, on leave of absence from the Institute of Physics, University of Mainz, Germany.

‡ Also a member of the Department of Biochemistry.

(1) Braum, R. M. *Chem. Eng. News* **1990**, *68* (44), 22–25.
(2) Ross, P. E. *Sci. Am.* **1991**, *264* (1), 114–116.
(3) Chang, A. H. H.; Ermler, W. C.; Pitzer, R. M. *J. Phys. Chem.*, in press.
(4) Haufler, R. E.; Conceicao, J.; Chibante, L. P. F.; Chai, Y.; Byrne, N. E.; Flanagan, S.; Haley, M. M.; O'Brien, S.; Pan, C.; Xiao, Z.; Billups, W. E.; Ciufolini, M. A.; Hauge, R. H.; Margrave, J. L.; Wilson, L. J.; Curl, R. F.; Smalley, R. E. *J. Phys. Chem.* **1990**, *94*, 8634–8636.
(5) Allemand, P.-M.; Koch, A.; Wudl, F.; Rubin, Y.; Diederich, F.; Alvarez, M. M.; Anz, S. J.; Whetten, R. L. *J. Am. Chem. Soc.* **1991**, *113*, 1050–1051.
(6) Lai, S.-T. F.; Evans, C. A., Jr. *Org. Mass Spectrom.* **1978**, *13*, 733–734.
(7) Maas, W. P. M.; Nibbering, N. M. M. *Int. J. Mass Spectrom. Ion Processes* **1989**, *88*, 257–266.
(8) Leiter, K.; Ritter, W.; Stamatovic, A.; Mark, T. D. *Int. J. Mass Spectrom. Ion Processes* **1986**, *68*, 341–347.
(9) Bowie, J. H.; Stapleton, B. J. *J. Am. Chem. Soc.* **1976**, *98*, 6480–6483.
(10) Compton, R. N. Negative Ion States. *NATO ASI Series C: Mathematical and Physical Sciences, Vol. 142, Photophysics and Photochemistry in the Vacuum Ultraviolet*; McGlynn, S. P., Findley, G. L., Huebner, R. H., Eds. D. Reidel: Boston, 1985; pp 270–271.
(11) Yannoni, C. S.; Johnson, R. D.; Meijer, G.; Bethune, D. S.; Salem, J. R. *J. Phys. Chem.* **1991**, *93*, 9–10.
(12) Spence, D.; Chupka, W. A.; Stevens, C. M. *Phys. Rev. A* **1982**, *26*, 654–657.
(13) Kroto, H. W.; Heath, J. R.; O'Brien, S. C.; Curl, R. F.; Smalley, R. E. *Nature* **1985**, *318*, 162–163.
(14) Heath, J. R.; O'Brien, S. C.; Zhang, Q.; Liu, Y.; Curl, R. F.; Kroto, W.; Tittel, F. K.; Smalley, R. E. *J. Am. Chem. Soc.* **1985**, *107*, 7779–7780.
(15) Kratschmer, W.; Lamb, L. D.; Fostiropoulos, K.; Huffman, D. R. *Nature* **1990**, *347*, 354–358.
(16) Aije, H.; Alvarez, M. M.; Anz, S. J.; Beck, R. D.; Diederich, F.; Fostiropoulos, K.; Huffman, D. R.; Kratschmer, W.; Rubin, Y.; Schriver, K. E.; Sensharma, D.; Whetten, R. J. *Phys. Chem.* **1990**, *94*, 8630–8633.
(17) Haufler, R. E.; Chai, Y.; Chibante, L. F. P.; Conceicao, J.; Jin, C.; Wang, L.-S.; Maruyama, S.; Smalley, R. E. *Mater. Res. Soc. Symp. Proc.* **1990**, *206*, in press.

0002-7863/91/1513-6795$02.50/0